Hybrid asynchronous absorbing layers based on Kosloff damping for seismic wave propagation in unbounded domains

Sijia Li, Michael Brun, Irini Djeran-Maigre, Sergey Kuznetsov

HYBRID ASYNCHRONOUS ABSORBING LAYERS BASED ON KOSLOFF DAMPING FOR SEISMIC WAVE PROPAGATION IN UNBOUNDED DOMAINS

Sijia Li[a] , Michael Brun[a] , Irini Djeran-Maigre[a] , Sergey Kuznetsov[b]

[a] *Univ Lyon, INSA-Lyon, GeoMaS, 69621Villeurbanne, France*

[b] *Institute for Problems in Mechanics, 119526 Moscow, Russia*

ABSTRACT

This paper presents a novel approach for modeling infinite media, called Hybrid (different time integrators) Asynchronous (different time steps) Kosloff Absorbing Layers with Increasing Damping (HA-Kosloff ALID). By using strong forms of wave propagation in Kosloff media, its design equation is derived as well as optimal conditions between physical and absorbing domains. Explicit/Implicit co-simulation is adopted to reduce computation time. Examples of semi-infinite bar and Lamb's test are implemented to illustrate the efficiency of our approach in terms of accuracy and CPU time, in comparison to Rayleigh ALID and PML. It turns out to be efficient and convenient for modeling unbounded domain.

Keywords: unbounded domains, wave propagation, subdomain decomposition, hybrid asynchronous time integration

1. INTRODUCTION

One of the critical points of the numerical simulation of wave propagation problems in unbounded domains using the finite element method is how to simulate infinite media. The simplest way is to consider a very large extended numerical mesh, but it leads to important computation times, in particular when long time duration excitations are considered. Hence, non-reflecting boundary conditions are required at the boundary of the truncated domain for mimicking infinite or semi-infinite media. Several kinds of artificial boundaries in numerical methods have been developed to avoid spurious waves reflected at the boundary, such as the infinite elements (Bettess [1], Houmat [2]), absorbing boundary conditions (Enquist et al. [3]), or PML (Perfect Matched Layers).

PML proposed by Bérenger [4] is becoming increasingly used for dealing with infinite media in the context of finite difference method, as well as in the finite and spectral element methods. The first implementations of PML were carried out according to a velocity-stress format, using mainly the finite difference method and a split procedure for the components of velocities with respect to the interface (Chew and Liu [5], Collino and Tsoga [6]). Basu and Chopra [7, 8] proposed an unsplit formulation of the PML, displacement-based and integrated in time using Newmark time integrators, suitable for time-domain elastodynamics modeled with a finite element approach. An explicit version of the PML in three-dimension (Basu [9]) was successfully implemented in the Finite Element codes LS-DYNA [10] and DIANA [11]. Although PML tends to be now considered as the most effective way to model infinite media, the PML implementation is not straightforward in a general purpose finite element software. Thus, more convenient techniques were recently developed in the finite element context, based on simple damping formulations such as the widely used viscous damping Rayleigh matrix. Semblat et al. [12] and Rajagopal et al. [13] introduced efficient absorbing conditions into commercial finite element codes, called Absorbing Layers using Increasing Damping (ALID), based on Rayleigh viscous damping matrix associated with an increasing damping ratio in the thickness of the absorbing region. Zafati et al. [14, 15] improved the ALID

capabilities of mimicking infinite media by tuning the material characteristics in the thickness of the ALID in order to minimize spurious reflections between sublayers related to increasing damping. One of the drawbacks of the viscous Rayleigh damping in FE software is its dependence with respect to frequencies in the problem. Consequently, it is interesting to explore the capabilities of other damping formulations than Rayleigh damping, while remaining very simple to be easily set up in a general FE software. Absorbing boundary based on a simple modification in the wave propagating equation, was proposed by D. Kosloff and R. Kosloff [16]: in Kosloff medium, the wave travels without changing shape and the wave amplitude decreases with distance at a frequency independent rate. Some similarities between PML and Kosloff absorbing boundary have been discussed by Carcione and Kosloff [17]. It was shown that in the case of SH waves, a modified Kosloff formulation matches the split formulation of the PML, before the spatial and time discretization, highlighting the relation between the two approaches. Here, the Kosloff damping formulation is explored with a view to setting up efficient and convenient absorbing layers for modelling infinite media. In addition, in FE implementation, if an explicit time integration scheme is adopted both in the domain of interest and in the absorbing region, the introduction of absorbing layer induces a decrease of the critical time step size [18]. As a result, the hybrid time integration capabilities are useful to integrate, in a decoupled manner, the domain of interest and the absorbing layer in such a way that the explicit time integration of the wave propagation is not affected by the choice of damping characteristics in the ALID. The resulting absorbing layer will be called Hybrid Asynchronous-Kosloff Absorbing Layers using Increasing Damping (HA-Kosloff ALID), because it employs Hybrid (different time integrators) Asynchronous (different time steps) Time Integrator developed by Combescure and Gravouil for Newmark time integrators [19, 20], and more recently, by Brun et al. [21] for more general time integrators such as the widely used Generalized-alpha schemes.

In this paper, the capabilities of the Kosloff formulation for damping are investigated to set up efficient HA-Kosloff ALID and compared with Rayleigh formulation. Firstly, the design of Kosloff absorbing layer is proposed by using the strong form of elastic wave propagation in Kosloff medium. The absorbing ability of Kosloff absorbing layer associated with a performance criterion is derived in the form of a logarithmic decrement and proved to be independent of frequency. A general formula for designing Kosloff absorbing layers using a multi-layer strategy is derived. In addition, optimal conditions are obtained to avoid the spurious waves reflected at the interface between physical domain and Kosloff absorbing layer domain. In the case of non-harmonic waves, Kosloff absorbing layer is found to be less sensitive to the design parameters in comparison to Rayleigh absorbing layer. Secondly, the weak formulation of the decomposed problem is given in order to derive the space discretization. Kosloff formulation turns out to have a very simple finite element expression which corresponds to two new matrices, similar to the mass matrix, operating on velocities and displacements in semi-discrete equation of motion. For the time discretization, the GC method proposed by Gravouil and Combescure, belonging to more general HATI methods, is employed in order to integrate the ALID with an implicit time integrator, letting unchanged the critical time step in the domain of interest handled with an explicit time integration. Finally, Lamb's test illustrates the efficiency of HA-Kosloff ALID in terms of accuracy and CPU time, in comparison to HA-Rayleigh ALID [14] and the HA-PML [22]. The differences among the approaches are analyzed to demonstrate the advantages and disadvantages of each approach.

2. STRONG FORM OF THE WAVE PROPAGATION IN A KOSLOFF MEDIUM

The design of Kosloff absorbing layer aims at damping out all the incident waves from the domain of interest while minimizing the spurious waves reflected at the boundary of the truncated

domain. For this purpose, using the strong form for the wave propagation in the Kosloff medium, the absorbing ability of Kosloff absorbing layer related to a target performance criterion will be quantified in the form of logarithmic decrement. The optimal conditions at the interface between a non-dissipative elastic medium Ω_1 and a dissipative Kosloff medium Ω_2 will be analytically established by considering the continuous problem of wave propagation.

2.1 Governing equations of a Kosloff medium

The governing equations in elastodynamics are modified by Kosloff and Kosloff [16] in order to introduce a specific damping, called in the following Kosloff damping. The displacement vector field $\underline{u}$ in the Kosloff medium is governed by the modified equations:

$$\rho\partial_t^2\underline{u} = \mathrm{div}\left(\underline{\underline{\sigma}}(\underline{u})\right) - 2\rho\gamma\partial_t\underline{u} - \rho\gamma^2\underline{u} \tag{1}$$

$$\underline{\underline{\sigma}} = \lambda \mathrm{tr}\left(\underline{\underline{\varepsilon}}(\underline{u})\right) + 2\mu\underline{\underline{\varepsilon}}(\underline{u}) \tag{2}$$

$$\underline{\underline{\varepsilon}} = \frac{1}{2}\left[grad(\underline{u}) + grad(\underline{u})^T\right] \tag{3}$$

Eqs. (1) to (3) constitute the strong form of the propagation in a Kosloff medium, σ, ε, λ, μ, ρ, γ being the stress matrix, strain matrix, Lamé's coefficients, the density and damping ratio, respectively. It can be seen that the strong form of the equation of motion, in Eq. (1), has been changed with two additional damping terms related to displacements and velocities. The other two equations correspond to the elastic constitutive relationship and the definition of the infinitesimal strain. It will be shown in the following that the induced damping enables us to damp out the amplitude of a propagating wave in a Kosloff medium, irrespective of its frequency.

2.2 1D wave propagation in a Kosloff medium

The argument is developed for 1D wave propagation problem by distinguishing the P-waves and the S-waves in their strong form, written as:

$$\rho\partial_t^2\underline{u} = (\lambda + 2\mu)\partial_x^2\underline{u} - 2\rho\gamma\partial_t\underline{u} - \rho\gamma^2\underline{u} \qquad P-waves \tag{4}$$

$$\rho\partial_t^2\underline{u} = \mu\partial_x^2\underline{u} - 2\rho\gamma\partial_t\underline{u} - \rho\gamma^2\underline{u} \qquad S-waves \tag{5}$$

By introducing harmonic solutions in its complex form $u(x,t) = u_0\exp(i(\omega_0 t - kx))$ into the above wave propagation equations, the expression of the wave number k can be obtained:

$$k = \frac{\omega_0}{v}\left(1 - i\frac{\gamma}{\omega_0}\right) \tag{6}$$

with the velocity v equal to $\sqrt{\frac{\lambda+2\mu}{\rho}}$ for P-wave and $\sqrt{\frac{\mu}{\rho}}$ for S-wave. The expression of the propagating wave in the 1D Kosloff medium is shown below,

$$u(x,t) = u_0\, exp(\, i(\omega_0 t - k_0 x))\, exp\left(-\frac{\gamma x}{v}\right) \tag{7}$$

The above expression confirms the fact that all the frequency components are equally attenuated due to the decay factor γ/v which is frequency independent as underlined by Carcione and Kosloff [17].

In order to design efficient absorbing layers based on the Kosloff damping, we assess the logarithmic decrement of the propagating wave. Using the previous expression in Eq. (7), the relationship between the logarithmic decrement is expressed as a function of the thickness Δx and the damping ratio γ of the Kosloff absorbing layer,

$$\delta = \ln\left(\frac{|u(x)|}{|u(x+\Delta x)|}\right) = \frac{\gamma \Delta x}{v_p} \tag{8}$$

It can be seen that the frequency wave ω_0 has no influence on the absorbing ability of Kosloff absorbing layer with regard to the logarithmic decrement, which means that all waves with all frequencies can be attenuated in the same way. In other words, Kosloff damping turns out to be independent of frequency. The velocity of P waves is higher than the velocity of S waves in the same medium. As a result, based on the above relationships, in order to reach the same logarithmic decrement, the necessary layer thickness for damping out S waves is smaller than the one related to P waves. In the following, the velocity of P waves v_p will be adopted for the design of absorbing layer so as to ensure that all the waves are attenuated according to the target decrement.

2.3 Optimal conditions at the interface between an elastic medium and a Kosloff medium

The wave propagation problem from an elastic medium to a Kosloff medium is considered below in the case of the 1D harmonic wave. Three components have to be taken into account: the incident wave u_1, the transmitted wave u_2, and the reflected wave u_R, as shown in Fig.1.

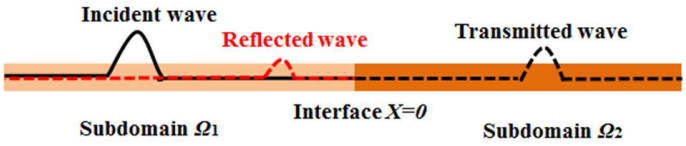

Fig.1 Wave propagation from elastic medium to Kosloff medium.

$$u_1(x,t) = A\,\exp[i\omega_0(t - \frac{x}{v_1})] \tag{9}$$

$$u_2(x,t) = T\,\exp[i\omega_0(t - \frac{x}{v_2})]\exp[-\frac{\gamma x}{v_2}] \tag{10}$$

$$u_R(x,t) = R\,exp[i\omega_0(t + \frac{x}{v_1})] \tag{11}$$

Based on the continuity of displacements and equilibrium of stresses at the interface, we can write:

$$u_2(x=0,t) = u_1 + u_R\,(x=0,t) \tag{12}$$

$$k_2\partial_x u_2(x=0,t) = k_1(\partial_x u_1 + \partial_x u_R)(x=0,t) \tag{13}$$

with k_1 equal to $\lambda_1 + 2\mu_1$ for P-waves or $2\mu_1$ for S-waves while k_2 equal to $(\lambda_2 + 2\mu_2)$ for P-waves or $2\mu_2$ for S-waves, where E_1 and E_2 are Young's moduli, ρ_1 and ρ_2 are the densities of subdomains Ω_1 and Ω_2, where $\lambda_1, \mu_1, \lambda_2, \mu_2$ are Lamé's coefficients in subdomain Ω_1 and Ω_2, respectively. The reflection coefficient $R_{interface}$ at the interface can be obtained as,

$$\frac{R}{A} = \frac{-\rho_2 v_2\left(1 - i\frac{\gamma}{\omega_0}\right) + \rho_1 v_1}{\rho_2 v_2\left(1 - i\frac{\gamma}{\omega_0}\right) + \rho_1 v_1} \tag{14}$$

By setting the ratio $\alpha = \frac{\rho_2 v_2}{\rho_1 v_1}$, the interface refection coefficient can be written:

$$\frac{R}{A} = \frac{1 - \alpha\left(1 - i\frac{\gamma}{\omega_0}\right)}{1 + \alpha\left(1 - i\frac{\gamma}{\omega_0}\right)} \tag{15}$$

If we want to reduce reflection at the interface, the modulus of the above complex valued reflection coefficient should be minimized. It leads to the following relationship:

$$\alpha = \frac{1}{\sqrt{1 + (\frac{\gamma}{\omega_0})^2}} \tag{16}$$

Now, we can give a simple condition on material properties of the Kosloff medium so as to cancel the reflected waves in the case of harmonic waves for P-waves and S-waves in 1D medium,

$$\begin{cases} E_2 = \dfrac{E_1}{1 + (\frac{\gamma}{\omega_0})^2} \\ \rho_2 = \rho_1 \\ \nu_2 = \nu_1 \end{cases} \tag{17}$$

where E_1 and E_2 are Young's moduli, ρ_1 and ρ_2 are the densities of subdomains Ω_1 and Ω_2, respectively. The above relationships show that, though the Kosloff medium is independent of frequency in terms of decrement, the optimal conditions at the interface depend on the frequency. Therefore, in the case of non-harmonic waves, there will be still some reflections at the interface. This is why we thoroughly evaluate in the following the effect of the chosen f_0 in terms of spurious reflections generated at the interface.

2.4Design of Kosloff absorbing layer using a multi-layer strategy

The Absorbing Layers using Increasing Damping (ALID), proposed by Semblat et al. [12], Rajagopal et al. [13] and improved by Zafati et al. [14], as shown in Fig.2, is considered by tuning the elastic parameters of each layer depending on the selected absorbing parameters as given by the optimal conditions in Eqs. (17). The main idea is to divide the Kosloff absorbing medium into several uniform layers, so that the decrements produced by each layer can be multiplied. Because of the logarithmic form of decrement, the total logarithmic decrement can be easily obtained. The evolution of damping ratio in layers has an important influence on the efficiency of the ALID. In this paper, a nonlinear increase of damping ratio is adopted to achieve a better accuracy.

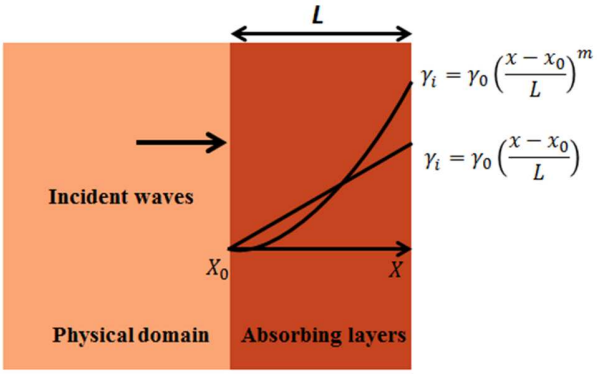

Fig.2 Evolution of the damping ratios in multi-layer absorbing subdomain

The parameters of each layer, indexed by (*i*) varying from 1 to N, which satisfies the optimal conditions at each interface, are given by:

$$\begin{cases} E_2^{(i+1)} = \dfrac{1+(\frac{\gamma_i}{\omega_0})^2}{1+(\frac{\gamma_{i+1}}{\omega_0})^2} E_2^{(i)} \\ E_2^{(1)} = \dfrac{1}{1+(\frac{\gamma_1}{\omega_0})^2} E_1 \\ \nu_2^{(i)} = \nu_1 \\ \rho_2^{(i)} = \rho_1 \\ \gamma_i = \gamma_0 \left(\dfrac{x_i}{L}\right)^m \end{cases} \tag{18}$$

where $E_2^{(i)}$ the Young's modulus, γ_i the damping ratio, $\nu_2^{(i)}$ Poisson's ratio, $\rho_2^{(i)}$ the density of each layer i in the subdomain Ω_2, ω_0 the chosen frequency to design absorbing layers, γ_0 the damping ratio in the last layer, m the power of the damping function, x_i the distance of each sublayer (i) from the interface of the ALID, varying according L the thickness of the ALID including all sublayers (i). By integrating the logarithmic decrement in Eq. (8) along the thickness of the ALID, and using the polynomial form of the damping parameter gamma in Eq. (18), the total logarithmic decrement δ can be assessed as:

$$\delta = \int_0^L \frac{\gamma_0}{v_\rho}\left(\frac{x}{L}\right)^m dx = \frac{\gamma_0 L}{(m+1)v_\rho} \tag{19}$$

The attenuation coefficient $R_{attenution}$for the system of absorbing layers is defined by:

$$R_{attenution} = \left(\frac{|u(x)|}{|u(x+\mathrm{L})|}\right)^2 = e^{-2\delta} \tag{20}$$

If the goal is to reach a target logarithmic decrement δ = ln(10), it means that 90% of the amplitude of the incident wave will be absorbed from the interface to the end of the ALID. Next, the attenuation also occurs for the reflection process from the end of the ALID towards the interface. Hence, the incident wave is attenuated by 99% and the attenuation coefficient $R_{attenution}$ is theoretically equal to 1% before the space and time discretization.

Finally, we can propose the general formula to design Kosloff absorbing layers based on the 1D harmonic wave problem in a Kosloff medium. After choosing the $R_{attenution}$, the total thickness L and the power m of the damping function, γ_0 can be obtained:

$$\gamma_0 = \frac{(m+1)}{2L} \times v_\rho \times \ln\left(\frac{1}{R_{attenution}}\right) \tag{21}$$

It is important to remark that the general formula to design Kosloff absorbing is similar to that of PML proposed by Collino and Tsogka [6], based on one-dimensional wave propagation ideas, β_0 is the damping parameter in the last PML layer.

$$\beta_0 = \frac{(m+1)}{2L} \times v_\rho \times \ln\left(\frac{1}{R_{attenution}}\right) \tag{22}$$

Indeed, the capabilities of the PML to damp out incident wave is very similar to the Kosloff damping but the behavior at the interface is different in the two cases, because it is well known the no reflection occurs at a PML interface for all the frequencies. This is not the case for Kosloff and Rayleigh damping as discussed in the next section.

2.5 1D non-harmonic wave propagation at the interface between an elastic medium and ALID: comparison between Rayleigh and Kosloff damping

In order to establish optimal condition at the interface, harmonic waves have been previously considered. The relationship shows that, though the Kosloff medium is independent of frequency in terms of decrement, the optimal conditions at the interface depend on the frequency. Therefore, in the case of non-harmonic waves, different reflections will occur at the interface, quantified by the interface reflection coefficient $R_{interface}$. We investigate the influence of the chosen frequency f_0 on the interface reflection coefficient $R_{interface}$ in the case of Kosloff damping. $R_{interface}$ related to Kosloff layer for another frequency f, which is different from f_0, has been derived from Eq. (15) as shown below:

$$R_{interface} = \frac{1 - \alpha\left(1 - i\frac{\gamma}{\omega_0}\frac{\omega_0}{\omega}\right)}{1 + \alpha\left(1 - i\frac{\gamma}{\omega_0}\frac{\omega_0}{\omega}\right)} \tag{24}$$

$$\alpha = \frac{1}{\sqrt{1 + (\frac{\gamma}{\omega_0})^2}} \tag{25}$$

For comparison purpose, the case of the Rayleigh damping is reminded and new insights will be provided for a relevant choice of the design frequency f_0. The design of Rayleigh ALID is written as:

$$\xi_0 = \frac{(m+1)}{2L\omega_0} \times v_\rho \times \ln(\frac{1}{R_{attenution}}) \tag{23}$$

which is only valid for harmonic waves due to the dependence of the Rayleigh damping on frequency. As a result, the attenuation coefficient $R_{attenution}$ has also to be assessed in the case of non-harmonic waves as a function of the chosen design frequency f_0. Here, it should be remarked that it is not the case of the Kosloff damping as shown by the previous design relation given in Eq. (21).

From the assumption adopted by the authors $\frac{\alpha_M}{\omega_0} = \alpha_K\omega_0 = \xi$[15], the form of the complex wave number is given by:

$$k_p(\omega) = \frac{\omega}{V_p}\sqrt{\frac{1 - \xi^2 - i\xi\left(\frac{\omega_0}{\omega} + \frac{\omega}{\omega_0}\right)}{1 + \xi^2\frac{\omega^2}{{\omega_0}^2}}} \tag{26}$$

The dimensionless imaginary part of $k_p(\omega)$ was proved to increase with increasing $\frac{\omega}{\omega_0}$, corresponding to the increase of the amplitude of the reflected wave [15]. It means that the high frequencies decay more quickly than the low frequencies. In other words, the relatively small f_0 can make more frequencies be attenuated over the $R_{attenution}$ defined by f_0 .Thus, it is beneficial to consider a relatively small f_0, in terms of absorbing ability for non- harmonic waves in Rayleigh absorbing layer.

For a given frequency f, the interface reflection coefficient $R_{interface}$ at an interface between an elastic medium and a Rayleigh medium designed at f_0 frequency is expressed as [15]:

$$R_{interface} = \frac{1 - \alpha\sqrt{1 + \xi^2 - i\xi\left(\frac{\omega_0}{\omega} - \frac{\omega}{\omega_0}\right)}}{1 + \alpha\sqrt{1 + \xi^2 - i\xi\left(\frac{\omega_0}{\omega} - \frac{\omega}{\omega_0}\right)}} \tag{27}$$

$$\alpha = \frac{1}{\sqrt{1 + \xi^2}} \tag{28}$$

The interface reflection coefficients $R_{interface}$ for Kosloff and Rayleigh cases are plotted in Figures 3 and 4 for a frequency ratio f/f_0. It can be remarked that, for the Kosloff damping, the interface reflection coefficient decreases when the frequency ratio increases. Thus, it advocates the choice of a design frequency f_0 less than the dominant frequency present in the investigated problem so as the frequency ratio increases, leading to a very low reflection coefficient. In the case of Rayleigh damping, same analysis can be conducted because small frequency ratio leads to much higher interface reflection coefficient than high frequency ratio. Consequently, taking into account the benefits of the relatively small frequency f_0 in terms of decrement for Rayleigh layer and in terms of interface reflection for both Kosloff and Rayleigh layers, one method to reduce the reflection for the case of non-harmonic waves is to define the f_0 relatively small.

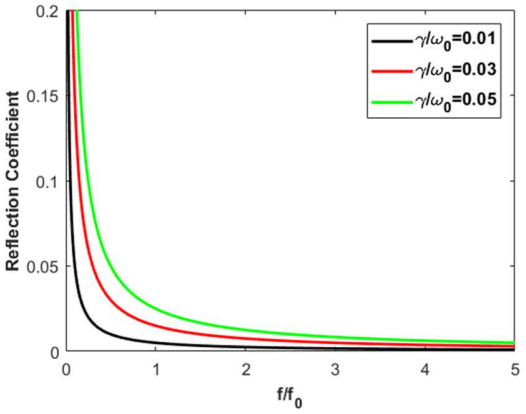

Fig.3 $R_{interface}$ for Kosloff using different f/f_0 and $\frac{\gamma}{\omega_0}$

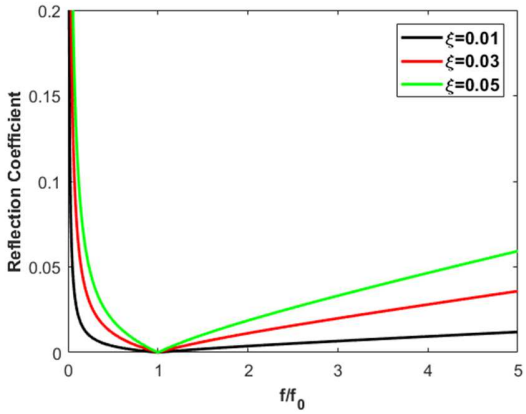

Fig.4 $R_{interface}$ for Rayleigh using different f/f_0 and ξ

Secondly, the figures also show that, with ξ and γ/ω_0 increasing, the interface reflection coefficient $R_{interface}$ increases in both figures. Due to the dependence of the absorbing ability on frequency in the case of Rayleigh damping, with a smaller chosen frequency f_0, the damping ratio ξ of Rayleigh layer based on the general design formula Eq. (23) will be bigger, so it leads to the increase of reflection for all the frequencies. Regarding Kosloff layer, a decreased design frequency f_0 gives a higher frequency-dependent damping parameter γ/ω_0. It implies that the chosen frequency should not be defined too small. As a result, a compromise has to be found to select a design frequency f_0 sufficiently small in comparison to the dominant frequency, without affecting to much the reflection coefficient. This will be verified in the following numerical investigations.

Finally, from the comparison between Figures 3 and 4, in the high frequency range, it can be highlighted that $R_{interface}$ related to the Kosloff damping is much less affected by the increase of the frequency-dependent damping parameter γ/ω_0 than the one related to the Rayleigh damping with increasing damping ratio ξ. The interface reflection coefficient tends to very low values for

Kosloff damping when frequency ratio increases, contrarily to Rayleigh damping. It is important because it means a better interface behavior of the Kosloff ALID than the Rayleigh ALID.

3. THE SPACE AND TIME DISCRETIZATION FOR HA-KOSLOFF ALID

The elastic wave propagation from an elastic non-dissipative medium to a dissipative medium should be discretized in space and time. In this paper, the hybrid time integration of the ALID based on Kosloff damping is presented.

Let Ω be a bounded domain belonging to $\mathbb{R}^2$ with a regular boundary. J= [0, T] is the time interval of interest. The domain Ω is divided into two partitions Ω_1 and Ω_2, as shown in Fig.5, such as: $\Omega_1 \cap \Omega_2 = \emptyset$ and $\partial\Omega_1 \cap \partial\Omega_2 = \Gamma$. Γ denotes the interface between the two subdomains, subdomain Ω_1 representing the non-dissipative medium (the domain of interest) and subdomain Ω_2 the Kosloff medium. The goal is to integrate the domain of interest Ω_1 using a conditionally stable explicit time integration scheme suitable for modeling the wave propagation, while integrating the Kosloff ALID with an unconditionally stable implicit time integration scheme in order to not decrease the size of the critical time step in Ω_1.

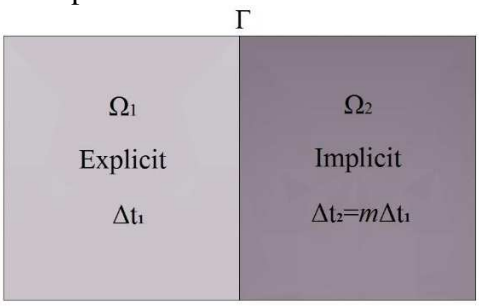

Fig.5 Domain Ω divided into two subdomains Ω_1 and Ω_2 with their material characteristics. Subdomain Ω_1 is handled by an explicit scheme with fine time step and subdomain Ω_2 by an implicit scheme with large time step

3.1 Weak form and space discretization

The subdomain Ω_1 is characterized by its density ρ_1, Young's modulus E_1, Poisson's coefficient ν_1, $\underline{b_1}$ the body force, $\underline{u_1^D}$ the Dirichlet prescribed displacement on Γ_1^D and $\underline{g_1^N}$ the traction force at the Neumann condition on Γ_1^N. The subdomain Ω_2 is characterized by its density ρ_2, Young's modulus E_2, Poisson's coefficient ν_2, $\underline{b_2}$ the body force, $\underline{u_2^D}$ the Dirichlet prescribed displacement on Γ_2^D, $\underline{g_2^N}$ the traction force at the Neumann condition on Γ_2^N and the Kosloff damping parameter γ introduced in the strong form of the wave equation in Eq. (1) .

In order to write the weak form of the coupled problem in Ω divided into two partitions Ω_1 and Ω_2 , test functions $\underline{v_1}$ and $\underline{v_2}$ belonging to the appropriate spaces W_1^* and W_2^* must be introduced :

$$\begin{cases} \underline{v_1} \in W_1^* , W_1^* = \left\{ \underline{v_1} \in \left(H^1(\Omega_1)\right)^d and\ \underline{v_1} = 0\ on\ \Gamma_1^D \right\} \\ \underline{v_2} \in W_2^* , W_2^* = \left\{ \underline{v_2} \in \left(H^1(\Omega_2)\right)^d and\ \underline{v_2} = 0\ on\ \Gamma_2^D \right\} \end{cases} \tag{29}$$

The solutions $\underline{u_1}$ and $\underline{u_2}$ belong to the appropriate spaces W_1 and W_2:

$$\begin{cases} \underline{u}_1(t) \in W_1, W_1 = \left\{ \underline{u}_1 \in \left(H^1(\Omega_1)\right)^d and\ \underline{u}_1 = u_1^D\ on\ \Gamma_1^D \right\} \\ \underline{u}_2(t) \in W_2, W_2 = \left\{ \underline{u}_2 \in \left(H^1(\Omega_2)\right)^d and\ \underline{u}_2 = u_2^D\ on\ \Gamma_2^D \right\} \end{cases} \tag{30}$$

where d is the space dimension (equal to 1, 2 or 3). According to a dual Schur approach, the introduction of the Lagrange multipliers allows us to glue the velocities of the two subdomains at the interface Γ [19, 20]. The Lagrange multipliers belong to the adapted dual trace space related to the interface between the two subdomains, denoted by Q. All the considered space variables are assumed to be sufficiently smooth and regular.

Next, using a dual Schur formulation, the principle of virtual power for transient dynamics can be written. Find the solution $\underline{u}_1(t) \in W_1$, $\underline{u}_2(t) \in W_2$ and $\underline{\lambda}(t) \in Q$, for which the following weak form is satisfied $\forall \underline{v}_1 \in W_1$, $\forall \underline{v}_2 \in W_2$ and $\forall \underline{\mu} \in Q$:

$$\int_{\Omega_1} \rho_1 \underline{v}_1 \cdot \ddot{\underline{u}}_1 d\Omega + \int_{\Omega_1} \underline{\underline{\varepsilon}}(\underline{v}_1) : \underline{\underline{\sigma}}_1 d\Omega + \int_{\Omega_2} \rho_2 \underline{v}_2 \cdot \ddot{\underline{u}}_2 d\Omega + \int_{\Omega_2} \underline{\underline{\varepsilon}}(\underline{v}_2) : \underline{\underline{\sigma}}_2 d\Omega + \int_{\Omega_2} 2\rho_2 \gamma \underline{v}_2 \cdot \dot{\underline{u}}_2 d\Omega + \int_{\Omega_2} \rho_2 \gamma^2 \underline{v}_2 \cdot \underline{u}_2 d\Omega + \int_{\Gamma_I} \underline{v}_1 \cdot \underline{\lambda} d\Gamma + \int_{\Gamma_I} \underline{v}_2 \cdot \underline{\lambda} d\Gamma + \int_{\Gamma_I} \underline{\mu} \cdot \left(\dot{\underline{u}}_1 - \dot{\underline{u}}_2\right) d\Gamma = \int_{\Omega_1} \underline{v}_1 \cdot \underline{b}_1 d\Omega + \int_{\Gamma_1^N} \underline{v}_1 \cdot \underline{g}_1^N d\Gamma + \int_{\Omega_2} \underline{v}_2 \cdot \underline{b}_2 d\Omega + \int_{\Gamma_2^N} \underline{v}_2 \cdot \underline{g}_2^N d\Gamma \tag{31}$$

where the stress tensor $\underline{\underline{\varepsilon}}_2$ satisfies the behavior law given in Eq. (2). Then, we follow the classical lines of the finite element discretization. At the interface between the subdomains, the continuity of velocities is imposed by the following condition:

$$L_1 \dot{U}_1 + L_2 \dot{U}_2 = 0 \tag{32}$$

where L_1 and L_2 are the Boolean matrices in the case of matching meshes at the interface; they operate on nodal vectors associated with the two subdomains Ω_1 and Ω_2; they pick out the degrees of freedom belonging to the interface Γ in order to ensure the kinematic continuity at the interface.

Thus, the restricted velocities at the interface can be obtained from the global nodal velocity vectors $\dot{U}_1$and $\dot{U}_2$ by the relationships:

$$\begin{cases} \dot{U}_1^\Gamma = L_1 \dot{U}_1 \\ \dot{U}_2^\Gamma = L_2 \dot{U}_2 \end{cases} \tag{33}$$

Same relationships hold for the global virtual nodal velocities V_1 and V_2. Finally, interface terms involving the Lagrange multiplier field can be expressed as:

$$\begin{cases} \int_{\Gamma_I} \underline{v}_1 \cdot \underline{\lambda} d\Gamma = V_1^T L_1^T \lambda \\ \int_{\Gamma_I} \underline{v}_2 \cdot \underline{\lambda} d\Gamma = V_2^T L_2^T \lambda \end{cases} \tag{34}$$

From the weak form of the global problem in Eq. (31), the semi-discrete equations in space can be derived, corresponding to the two equations of motion related to the two subdomains, completed with a kinematic condition. In the following, the hybrid integration of this set of equations will be carried out in order to propose a hybrid asynchronous Kosloff ALID.

3.2 Time discretization of the Hybrid Asynchronous absorbing layers

For the time discretization, the GC method proposed by Gravouil and Combescure is employed [19, 20]. Adopting the continuity of velocities at the interface, it was demonstrated that the coupling GC method is stable for any Newmark integrators (implicit and explicit) with their own time step depending on subdomains. As illustrated in Fig.5, an explicit time integrator with a fine time step

Δt_1 is adopted for the subdomain Ω_1 and an implicit time integrator with a large time step Δt_2 is used for subdomain Ω_2 , with $\Delta t_2 = m\Delta t_1$, m being the time step ratio between two subdomains. In this way, hybrid (different schemes associated) asynchronous (different time steps depending on subdomains) absorbing layers can be obtained. The equilibrium of subdomain 2 is prescribed at time t_m at the end of the large time Δt_2, while the equilibrium of subdomain 1 is prescribed at every time $t_j = j\Delta t_1$ (j =1, 2...m) at the fine time scale. The gluing of the velocity at the interface is written at the fine time scale.

Using the GC method, the wave propagation can be simulated using a fine time step, without being affected by the specific formulation adopted for the absorbing region at the boundary of the truncated mesh. Moreover, the multi-time step capabilities enable us to build efficient absorbing region in terms of computation time.

Finally, the weak form given in Eq. (31) with the velocity continuity equation in Eq. (32) and the expression of the interface terms as a function of the Lagrange multipliers in Eq. (34), can be expressed in the following discrete form in space and time:

$$\mathrm{M}_1\ddot{\mathrm{U}}_1^{\mathrm{j}} + \mathrm{K}_1\mathrm{U}_1^{\mathrm{j}} = \mathrm{F}_1^{\mathrm{ext,j}} - \mathrm{L}_1^{\mathrm{T}}\lambda^j \quad \text{at time } t=t_j \tag{35}$$

$$M_2\ddot{U}_2^m + C_1\dot{U}_2^m + C_2U_2^m + K_2U_2^m = F_2^{\mathrm{ext,m}} - L_2^T\lambda^m \quad \text{at time } t=t_m \tag{36}$$

$$L_1\dot{U}_1^j + L_2\dot{U}_2^j = 0 \quad \text{at time } t=t_j \tag{37}$$

$$C_1 = \sum 2\int_\Omega \rho\gamma \quad [N^e]^T[N^e]d\Omega \tag{38}$$

$$C_2 = \sum \int_\Omega \rho\gamma^2[N^e]^T[N^e]d\Omega \tag{39}$$

where N^e is the shape function matrix associated with the element indexed by *e*, belonging to the subdomain Ω_2. Here, we can see that Kosloff formulation turns out to have a very simple finite element expression which corresponds to two new matrices, similar to the mass matrix, operating on velocities and displacements in semi-discrete equation of motion. The first equation is the discrete equation of motion of subdomains Ω_1 written at time t_j (fine time scale), whereas the second equation is the discrete equations of motion of subdomains Ω_2 written at time t_m (large time scale). On right hand side of the above equations, the interface forces enable the subdomains to be glued at their interface Γ. The third equation is the velocity continuity.

Newmark time integration schemes [23] are adopted for the time discretization, characterized by the parameters γ_2=0.5 and β_2=0.25 for the implicit time integration (Constant Average Acceleration scheme) and the parameters γ_1=0.5 and β_1=0 for the explicit time integration scheme (Central Difference scheme). By introducing the approximate Newmark formulae, it leads to the equations of motion written as:

$$\widetilde{M}_1\ddot{U}_1^j = F_1^{\mathrm{ext,j}} - K_1U_1^{j-1,p} - L_1^T\lambda^j \tag{40}$$

$$\widetilde{M}_2\ddot{U}_2^m = F_2^{\mathrm{ext,m}} - C_1\dot{U}_2^{0,p} - C_2U_2^{0,p} - K_2U_2^{0,p} - L_2^T\lambda^m \tag{41}$$

where $U_1^{j-1,p}$ and $\dot{U}_2^{0,p}$ denote the predictor values in terms of displacement and velocity, classically introduced in approximate Newmark formula; they correspond to quantities known at the beginning of the fine step and of the large time step, respectively.

The effective stiffness matrices $\widetilde{M}_1$ and $\widetilde{M}_2$ related to the two subdomains are defined by:

$$\widetilde{M}_1 = M_1 + \beta_1\Delta t_1^2K_1 \tag{42}$$

$$\widetilde{M}_2 = M_2 + \beta_2\Delta t_2^2(K_2 + C_2) + \gamma_2\Delta t_2C_1 \tag{43}$$

The kinematic quantities are divided into two parts: the free and the linked quantities in the coupling GC method. The free quantities are calculated by taking into account the internal and

external forces, without considering the interface forces, whereas the linked quantities are obtained from the interface loads given by the Lagrange multiplier vector λ.

It was demonstrated that the kinematic continuity condition can be expressed as a reduced-size interface problem as follows:

$$H\lambda^j = b_j \tag{44}$$

with the interface operator and the right-hand side member vector defined by:

$$\begin{cases} H = \gamma_1 \Delta t L_1 \widetilde{M}_1^{-1} L_1^T + \gamma_2 \Delta t L_2 \widetilde{M}_2^{-1} L_2^T \\ b_j = L_1 \dot{U}_1^{\text{free},j} + L_2 \dot{U}_2^{\text{free},j} \end{cases} \tag{45}$$

The interface operator H is called the Steklov-Poincaré operator which can be viewed as the condensed effective stiffness matrix on the degrees of freedom belonging to the interface between the two subdomains. The right hand-side vector b_j only depends on the free velocities computed in both subdomains without considering the interface forces; it can be seen as a predictor value projected to the degrees of freedom belonging to the interface.

Finally, once derived the Lagrange multiplier vector, the quantities related to the interface forces can be computed and the time step is completed by summing these linked quantities to the free quantities previously obtained.

4. NUMERICAL APPLICATIONS

4.1 Numerical models with different chosen f_0

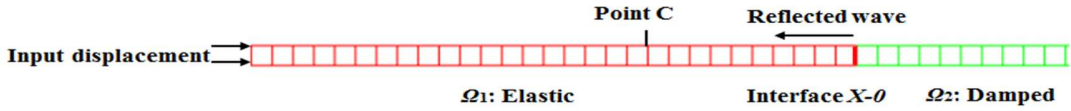

Fig.6 Numerical model of a semi-infinite elastic bar subjected to horizontal displacement

In order to explore the influence of the chosen frequency f_0 on the effectiveness of absorbing layers based on Kosloff and Rayleigh damping, numerical models of a semi-infinite elastic bar subjected to horizontal displacement at the free end, are established as shown in Figure 6. Thus, it simulates the propagation of *P* waves from a non-dissipative elastic medium to a dissipative medium. The simulation is conducted by using a homogeneous time step in both subdomains, the elastic subdomain is integrated in time with an explicit scheme and the subdomain related to the absorbing layer with an implicit scheme. On the basis of the general design formulas given in Eqs. (21, 23), we set the following parameters: $R_{attenution}$ equal to 0.01 (1% of reflection coming from the end of the absorbing layer), m equal to 2, and the size of the absorbing layer is kept as a constant, equal to 500m. As previously discussed in section 2.5, we will study the propagating P-wave for different chosen design frequencies f_0, or equivalently, for design periods T_0=1/f_0. The soil is assumed to be linear elastic with the following material characteristics: ρ_1=1700kg/m3, E_1=10MPa and ν_1= 0.24. The velocity of P-waves C_p is 83m/s. The model is composed of a soil subdomain with a size of 2000m. The recording point is located at 1750m from the left end of the model in order to facilitate the distinction between the wave reflection at the interface and the wave reflection coming from the end of the absorbing layer. Non-harmonic waves are investigated by considering a Ricker incident wave defined by:

$$Ric(t, t_p, t_s) = A\left(2\pi^2 \frac{(t-t_s)^2}{t_p^2} - 1\right) \exp\left(-\pi^2 \frac{(t-t_s)^2}{t_p^2}\right) \quad (46)$$

The Ricker wave plotted in time domain and in frequency domain in Figure 7, has three parameters: the fundamental period t_p, the time shift t_s and the amplitude A. The chosen values are: t_p=3s, t_s=3s and A =1. The fundamental period giving the dominant period of the present waves in the problem, the design period T_0 should be chosen higher than the dominant period so as to improve the behavior of the absorbing layer in terms of wave reflections as discussed previously. It is equivalent to choose the design frequency f_0 less than the dominant Ricker frequency 1/ t_p equal to 0.33 Hz.

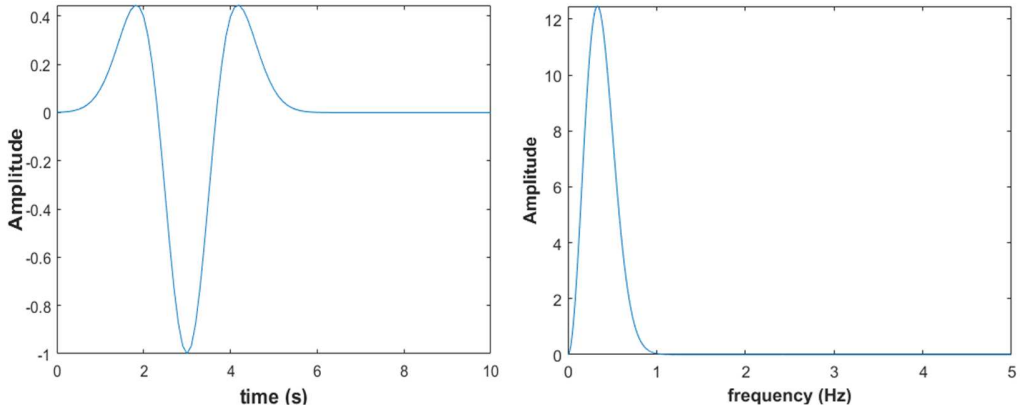

Fig.7 Waveform and Fourier transform of the Ricker wavelet

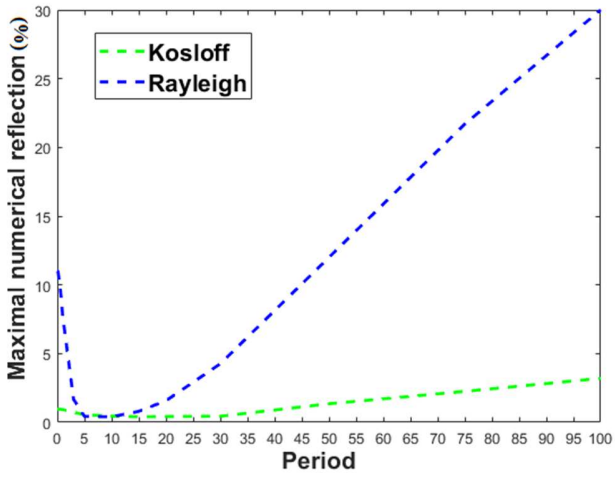

Fig.8 Maximal numerical reflection with different chosen periods T_0 (s).

The maximal numerical reflection coefficients for different design period T_0 are compared in Figure 8 for Kosloff and Rayleigh layers. It is clearly highlighted that the numerical reflection of Kosloff absorbing layer is always acceptable with different period changing from 0.01s to 100 s. On the contrary, the choice of the design period in the case of Rayleigh damping is much more sensitive

than the one in the case of Kosloff damping. For Kosloff damping, the best result corresponding to 0.4% of reflection is obtained for a design period of 15 s, which is much larger than the Ricker dominant period equal to 3 s. For Rayleigh damping, the lowest value of the reflection coefficient equal to 0.4% is obtained at the design period T_0 of 10s. Here, it has been confirmed that the relatively smaller value f_0 leads to better results.

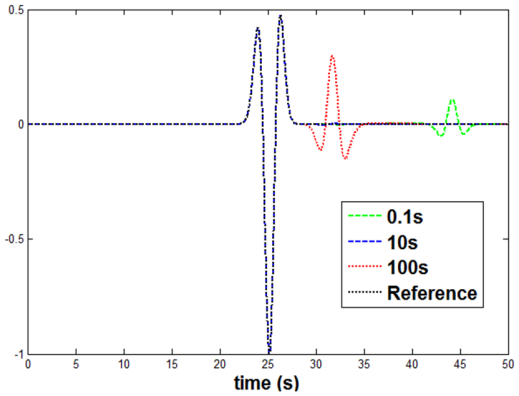

Fig.9 Horizontal displacement at point C for Rayleigh with different chosen periods

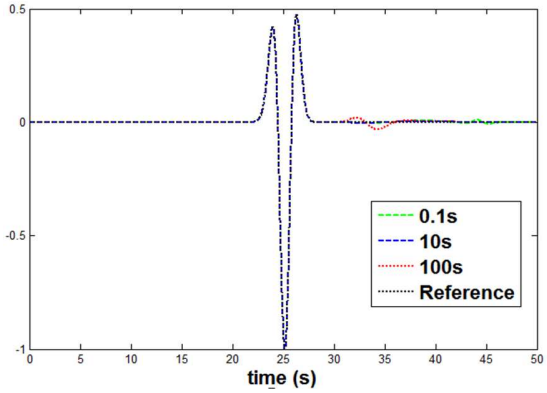

Fig.10 Horizontal displacement at point C for Kosloff with different chosen periods

Next, we will investigate where the maximal reflection comes from. The complete time history of the wave propagation at the point of observation for the design periods T_0 equal to 0.1s, 10s, 100s is shown in Figure 9 for Rayleigh absorbing layer and Figure 10 for Kosloff absorbing layer. The observed wave reflection includes both the reflected waves coming from the interface, characterized by the previously discussed ratio $R_{interface}$, and from the end of the absorbing layer, characterized by the ratio $R_{attenuation}$ used for the design of the absorbing layers.

As shown in Figures 9 and 10, for a design period equal to 10s which is higher than the dominant period of the problem (t_p equal to 3s), or equivalently, for a design frequency f_0 smaller than the the dominant frequency of the problem, both layers provide good results as expected. Next, we discuss the extreme cases: a very low value of the design period and a very high value of the design period.

For design period equal to 0.1s, corresponding to a frequency equal to 10 Hz which is much higher than the dominant frequency of the investigated problem (0.33 Hz), there will be more frequencies which will decay less than the $R_{attenution}$ defined by f_0. It leads to the increase of reflection from the end of absorbing layer. With the velocity of P-waves C_p equal to 83 m/s in this model, the reflection coming from the end of the ALID, arrives at the point of observation at 39 s, as observed in Fig. 9 for Rayleigh layer. With regard to Kosloff, the design frequency has no influence on the attenuation coefficient because of the independence of Kosloff in terms of decrement, with a high frequency, Kosloff layer still can obtain a good accuracy less than 1%, as shown in Figure 10.

For design period equal to 100 s, corresponding to a frequency equal to 0.01 Hz which is much lower than the dominant frequency of the problem, it leads to the increase of reflection at the interface $R_{interface}$for all the frequencies. Taken into account the P-wave velocity of 83m/s in this model, the reflection coming from the interface arrives at the point of observation at 27 s, for both Kosloff and Rayleigh layers in Figures 9 and 10. However, it can be noted that the influence of chosen design frequency on the reflection at the interface for Kosloff is much less than for Rayleigh, as previously shown in section 2.5 by the $R_{interface}$. As a conclusion, the interface behavior can be

clearly improved by the introduction of the Kosloff damping in comparison to the Rayleigh damping when low design frequency is selected.

In brief, in the case of Rayleigh layer, if the spectrum range of the incident wave is close to the dominant frequency, with an appropriate design chosen frequency, the waves will penetrate the Rayleigh medium with small reflections from the interface and from the end. However, for the waves which have a broad frequency range, it is more difficult to choose an appropriate design frequency f_0. It is explained first, by the fact that the absorbing ability of Rayleigh medium, characterized by $R_{attenution}$, depends on frequency, and second, by the sensitivity of the amount of spurious reflections at the interface, characterized by $R_{interface}$, to the design frequency f_0. On the contrary, the absorbing ability of the Kosloff damping is independent of frequency ($R_{attenution}$), and concerning the interface reflection ($R_{interface}$), Kosloff damping is less sensitive than Rayleigh damping. Hence, Kosloff layer better deals with broad frequency range waves in comparison to Rayleigh layer.

4.2 Lamb's test

In order to evaluate the effectiveness of hybrid asynchronous Kosloff absorbing layers, Lamb's test has been simulated. In Lamb's test, the concentrated load applied to the surface of an infinite half space medium generates three types of waves propagating through the soil, involving P, S waves and Rayleigh waves [24]. Consequently, Lamb's test can be considered as a good test for assessing the performance of absorbing layer. Non-harmonic waves are investigated by considering a Ricker incident waves as used in section 4 with the chosen values t_p=3s, t_s=3s and A =1MN.

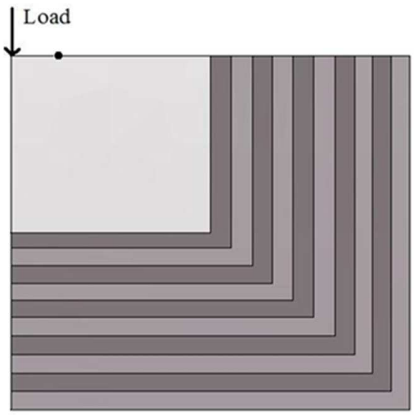

Fig.11 Lamb's test: the soil is integrated in time with explicit scheme (CD) and absorbing layers with implicit scheme (CAA)

In this section, Lamb's test is conducted by setting up HA- Kosloff ALID. Results obtained from HA- Rayleigh ALID and HA-PML based on the PML formulation proposed by Basu and Chopra [7, 8] are also calculated for comparison purpose. The soil is integrated in time with an explicit scheme and the ALID with an implicit scheme in order to avoid the critical time step in the soil partition to be affected by the introduction of the damping layers [14]. As illustrated in Figure 11, the numerical model for three different absorbing layers is the same, composed of a bounded soil (subdomain 1) with a size of 250m and absorbing layers (subdomain 2) with the thickness of 250m. The ALID design, given in Eq. (21), employed the following parameters: $R_{attenution}$ equal to 0.01, m equal to 2 and a design frequency f_0 equal to 0.1 Hz, chosen less than the Ricker dominant frequency equal to $1/t_p$=0.33 Hz. A recording point is located at 20m from the loading point on the surface.

In the case that an homogeneous time step satisfying the CFL condition applied in both subdomains, the vertical and horizontal displacements of three numerical models at the observation point are shown in Figures 12 and 13. We can observe that PML is the most precise, the reflected spurious wave being 0.27%, in terms of the vertical displacement, and 0.81% in terms of the horizontal displacement. In comparison, the reflected spurious waves of Kosloff and Rayleigh are in the same level with the chosen frequency f_0 equal to 0.1Hz. With respect to the vertical displacement, the reflected spurious wave is 1.38% for Kosloff and 1.51% for Rayleigh. With respect to the horizontal displacement, the reflected spurious wave is 0.94% for Kosloff and 1.15% for Rayleigh. Thus, it has shown that behavior of the Kosloff absorbing layer is very satisfactory for 2D non-harmonic waves composed of body and surface waves.

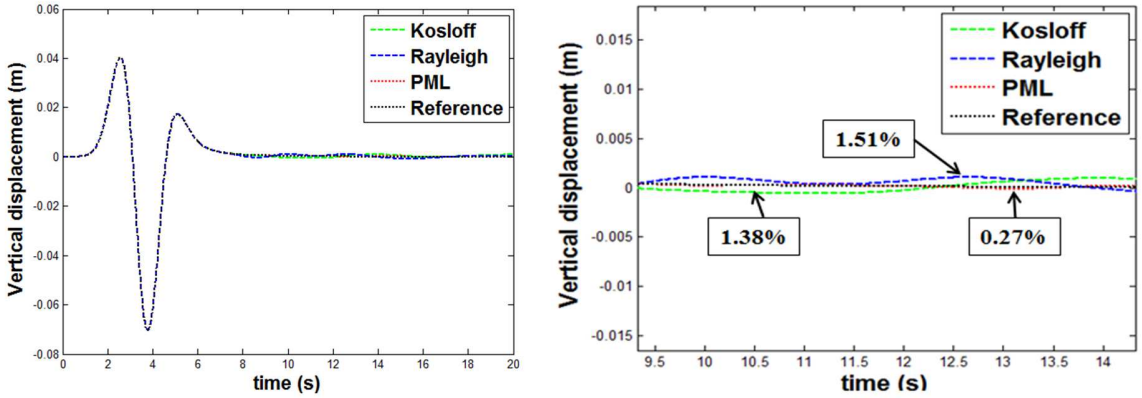

Fig.12 Vertical displacements at the observation point using different methods

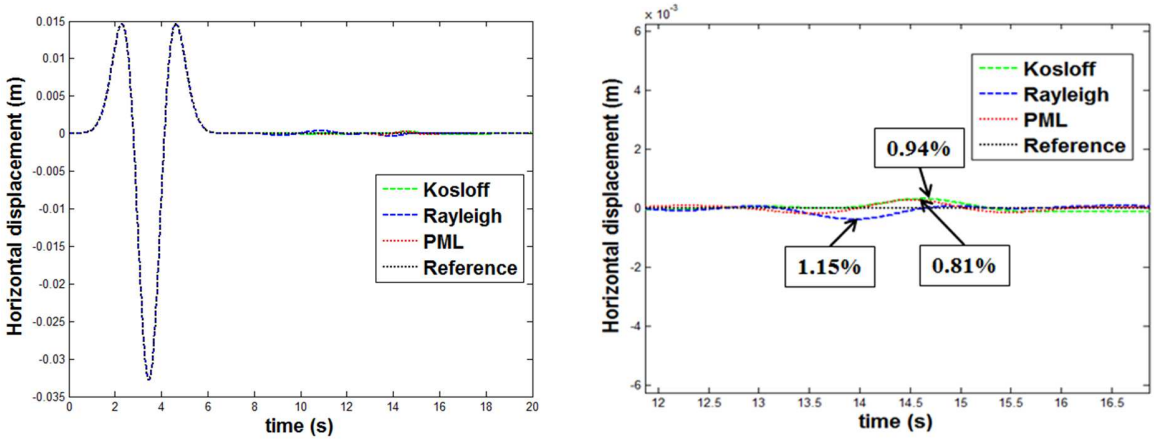

Fig.13 Horizontal displacements at the observation point using different methods

The kinetic and internal energies of the soil domain are computed for different absorbing layers as shown in Fig.14. The reference results are computed from an extended mesh in comparison to Figure 11, by keeping the same characteristics of the previous models (finite element size, material and loading characteristics). From Figure 14, all results are very close between each other. Then, in order to distinguish the difference between the different results, the L_2 norm error in time is computed between energies for different absorbing layers. Considering a quantity E over the time interval [0, T], the L_2 norm is defined by:

$$err = \frac{\left\| E^{(m)} - E_{\text{ref}} \right\|_{L^2([0,T])}}{\left\| E_{\text{ref}} \right\|_{L^2([0,T])}} \tag{47}$$

$E^{(m)}$ is the kinetic or internal energy obtained by different absorbing layers and E_{ref} is the reference energy obtained from the extended mesh. From Table.1, it can be observed that the errors are small for three types of absorbing layers. The errors of Kosloff and PML are clearly smaller than the errors of Rayleigh, because their absorbing capabilities are independent of frequency and better behavior at the interface.

Table.1 Relative errors of different methods

	Kinetic energy	**Internal energy**
Kosloff	0. 12%	0.08%
Rayleigh	0.58%	0.25%
PML	0.15%	0.10%

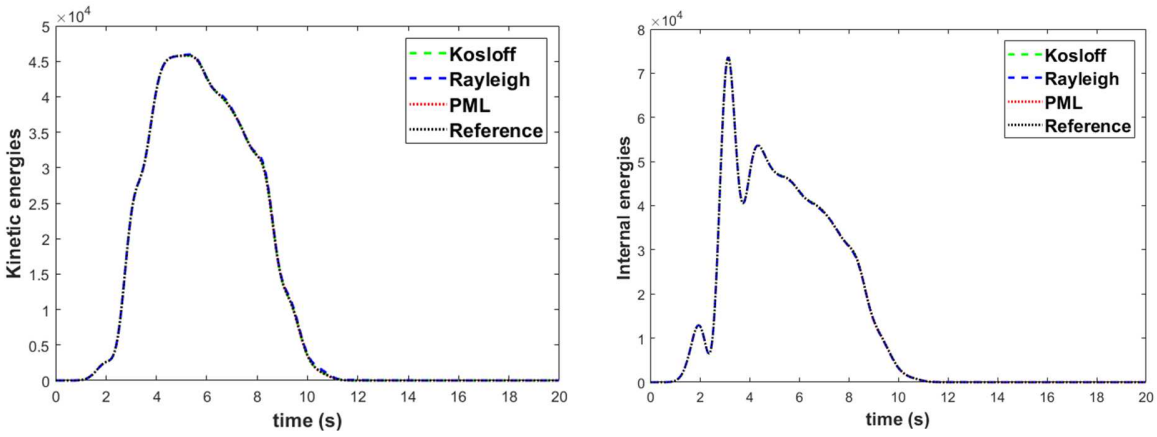

Fig.14 Kinetic and internal energies computed using different methods

The CPU times are given in Table.2 in a normalized form divided by CPU time of Kosloff layers. It can be concluded that, for the same numerical model, Kosloff layers and Rayleigh layers require almost the same CPU time. PML is more complex, so it takes more CPU time.

Table.2 Normalized CPU Time for different methods

	CPU time
Kosloff	1.00
Rayleigh	1.02
PML	1.39

4.3 Effect of the time ratio

Using the implicit time integration for the absorbing subdomain, we avoid the decrease of the critical time step in the explicit framework due to the introduction of damping into the discrete equation of motion. Moreover, as explained in section 3, it is possible to use a larger time step in the absorbing subdomain, because we use an unconditionally stable implicit scheme. The influence of

heterogeneous time steps on the accuracy is investigated. The subdomain soil is integrated with a central difference scheme (CD) with a fine time step, whereas absorbing layers are dealt with a constant average acceleration (CAA) scheme associated with a large time step in order to reduce the computation time in the absorbing layers. The horizontal and vertical displacements of the observation point for different absorbing layers with different time step ratios m ($\Delta t_2 = m\ \Delta t_1$) equal to 1, 5 and 10, are shown from Figure 15 to Figure 20. In terms of vertical displacements, the reflections of Kosloff and Rayleigh remain low with an increasing time step ratio m. It is not the case for PML, for which we observe increasing spurious reflections with the increase of the time step ratio m, with, for example, the amplitude of the reflected wave varying from 0.27% to 2.5% with respect to the vertical amplitude of the incident wave.

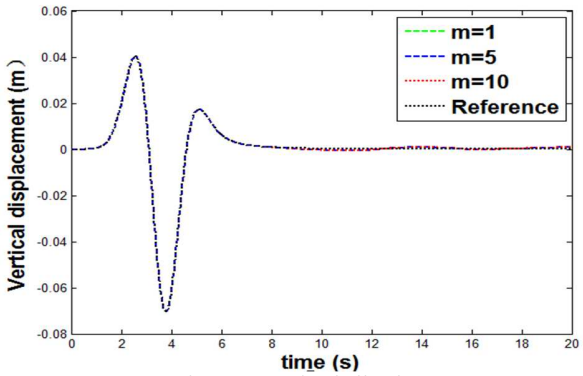

Fig.15 Vertical displacements for Kosloff using different time step ratios

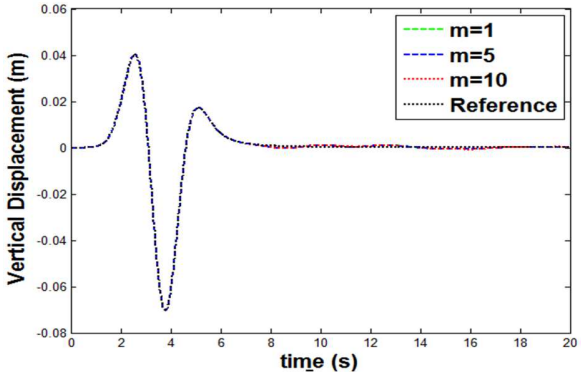

Fig.16 Vertical displacements for Rayleigh using different time step ratios

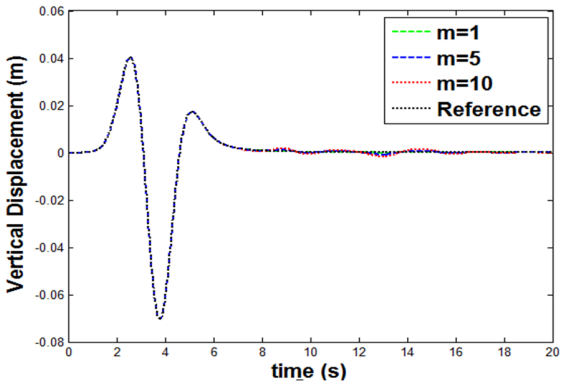

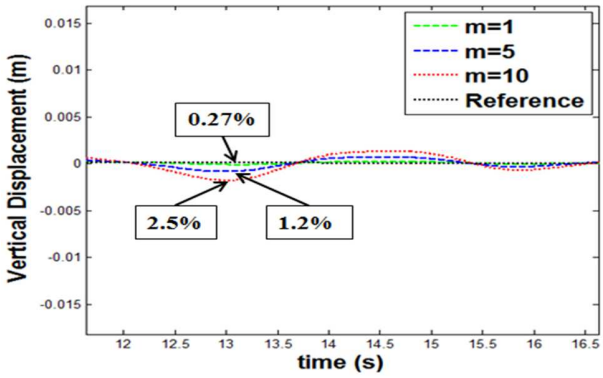

Fig.17 Vertical displacements for PML at the observation point using different time step ratios m

For horizontal displacements, it can be observed that, in comparison to the displacements given by reference results, the vertical amplitude of the spurious wave for Kosloff varies from 0.94% to 1.92% with respect to the horizontal amplitude of the incident wave. It can be seen that the HA-Kosloff ALID performs slightly better than HA- Rayleigh ALID, with spurious wave amplitude varying from 1.15% to 2.06%. For PML, the reflections increase from 0.81% to 6.06%, confirming the sensitivity of the HA-PML with the time step ratio in comparison to the HA-Kosloff ALID and HA- Rayleigh ALID.

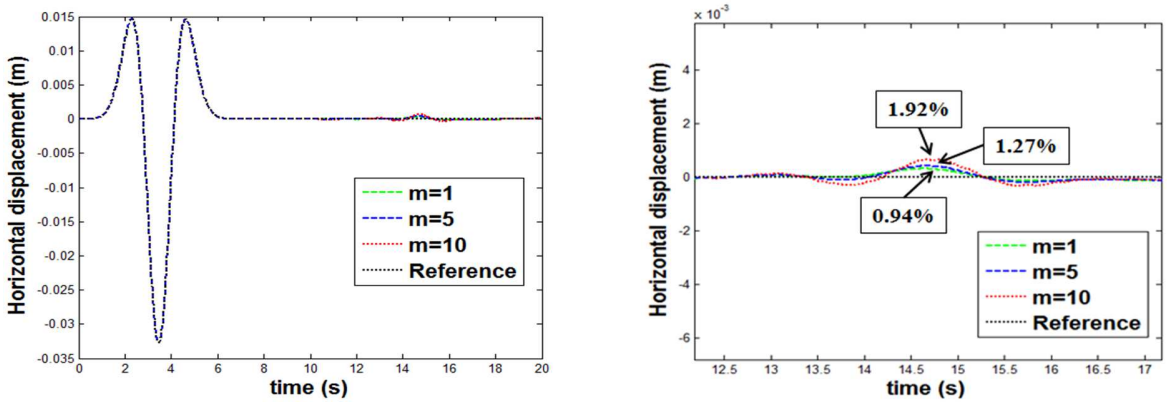

Fig.18 Horizontal displacements for Kosloff at the observation point using different time step ratios m

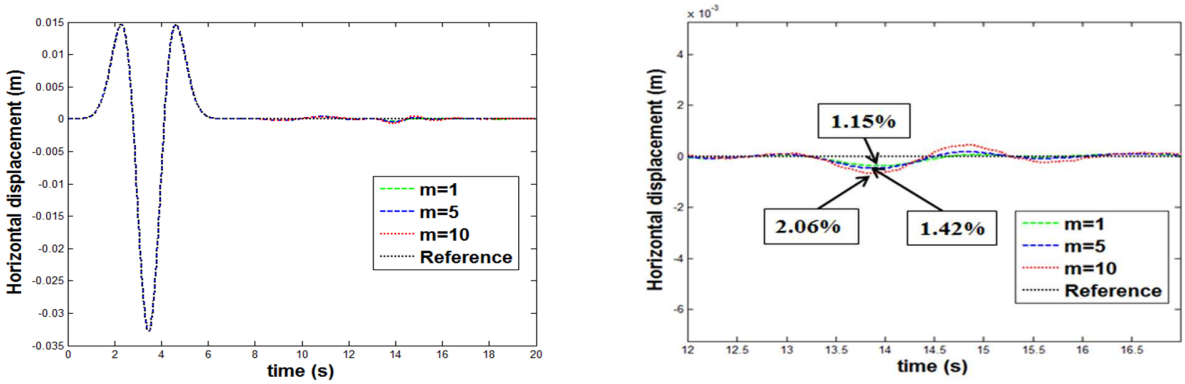

Fig.19 Horizontal displacements for Rayleigh at the observation point using different time step ratios m

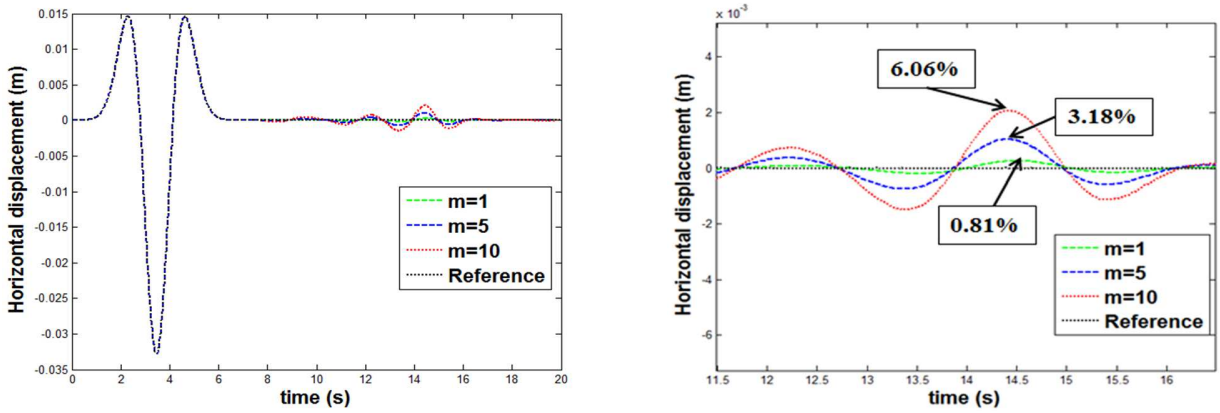

Fig.20 Horizontal displacements for PML at the observation point using different time step ratios m

The CPU times are resumed in Table.3 in a normalized form, that is divided by CPU time of the HA- Kosloff ALID for different time step ratios m. It shows that, with increasing different time step ratio, the CPU times related to the different absorbing layers decrease significantly, highlighting the strong interest of the hybrid asynchronous time integration. It implies that using explicit/implicit co-computation, not only the critical time step in the soil partition is not affected by the introduction of damping layer, but also large time steps can be adopted in absorbing layer domain to reduce the computation time.

Table.3 Normalized CPU Time for different methods using different time step ratios m

	Kosloff	Rayleigh	PML
m=1	1.00	1.02	1.39
m=5	0.44	0.46	0.70
m=10	0.36	0.40	0.58

The observed decrease of accuracy as the time step ratio increases, for all the previously investigated absorbing layers, can be explained by the following points. Firstly, the GC coupling algorithm is known to be dissipative as soon as heterogeneous time steps are used between the subdomains, generating spurious waves at the interface. It has been demonstrated that for GC method, when adopting the same time step, second order of accuracy is achieved and it leads to the first order of accuracy when adopting different time steps due to a slight spurious dissipation at the interface [20, 21]. Secondly, the reason why the accuracy of PML decreases more strongly than in the cases of Rayleigh and Kosloff damping can be found in Basu and Chopra's formulation [7-9], also adopted by commercial finite element codes LS-DYNA [10] and Diana [11]: one additional relationship was required to calculate the strain rate , $\dot{\varepsilon}(t_n) \approx (\varepsilon_n - \varepsilon_{n-1})/\Delta t_2$, Δt_2 being the time step in PML subdomain. As the time step increases, the error produced by this assumption may increase.

In order to confirm this last point, additional implicit–implicit co-simulations with homogeneous time steps (same time step in both subdomains), have been carried out. In such a way, the influence of heterogeneous time steps in the results is avoided and the time step can be increased while maintaining the stability of the co-simulation, because of the unconditional stability of the implicit time integration scheme. Both subdomains (soil and absorbing layers) are integrated with a constant average acceleration scheme (CAA) associated with the same time step, increasing from 0.025s to 0.25s depending on co-simulations, that is from a value corresponding to the CFL condition to a value ten times bigger. Maximal horizontal and vertical reflections for different absorbing layers are plotted in Figure 21. It can be seen that the reflections of Kosloff and Rayleigh hardly grow, with an increasing homogeneous time step in both subdomains. On the contrary, the horizontal and vertical reflections of PML quickly grow and become bigger than the reflections of Kosloff and Rayleigh cases. It can be concluded that, when the time step increases, the PML based on Basu and Chopra's formulation [7, 8] turns out to be less precise.

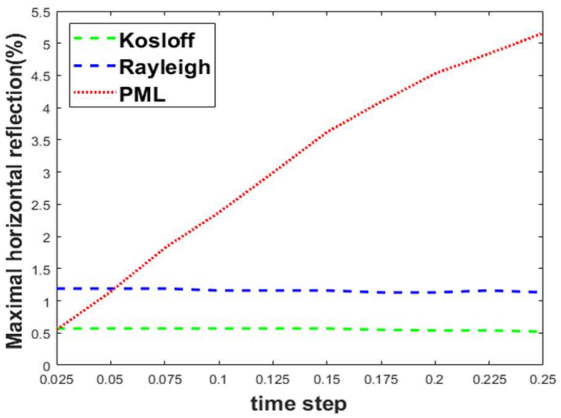

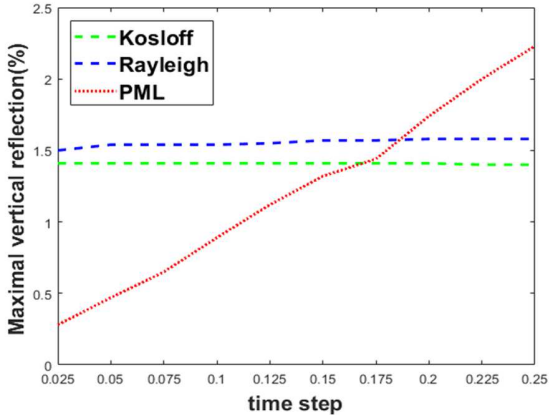

Fig.21 Maximal horizontal and vertical reflections for PML at the observation point for different homogeneous time steps (s) using implicit-implicit co-simulations

Overall, PML is the most accurate absorbing layer for a time step size close to the CFL condition and has the strong advantage to not require a design frequency as done in Kosloff and Rayleigh absorbing layers. However, it is more complex to be implemented in finite element software and it is observed that HA- PML produces more reflection with the increase of the time step ratio m. Kosloff absorbing layer is independent of frequency in terms of decrement and less sensitive to the influence of the chosen frequency f_0 at the interface in comparison to Rayleigh absorbing layer. In addition, the implementation of Kosloff damping in a finite element code is straightforward and the computation is quicker in comparison to the PML. Moreover, HA-Kosloff ALID is more accurate than HA- PML as the time step ratio increases. Therefore, Kosloff can be an alternative of PML to treat wave propagation problems.

5. CONCLUSION

In this paper, a new version of absorbing layer for modeling unbounded domain using finite element approach has been proposed on the basis of a specific damping formulation proposed by D. Kosloff and R. Kosloff [13]. Indeed, an interesting feature of the Kosloff damping for setting up efficient absorbing layers lies in its frequency independence. From the strong form of the wave propagation problem, optimal conditions at the interface between two media (elastic and Kosloff media) have been given as well as design equations for setting up the Kosloff absorbing layers. The advantages of the Kosloff damping have been highlighted in comparison to the classical Rayleigh damping, commonly available in general purpose finite element codes. Then the absorbing region has been integrated in time with an implicit Newmark time integration scheme with a large time step, independently of the explicit time integrator with fine time step adopted in the domain of interest. It leads to the proposition of a new version of absorbing layers, called Hybrid Asynchronous – Kosloff Absorbing Layers with Increasing Damping (HA-Kosloff ALID), and that is much more convenient to implement in a finite element code than PML techniques. Moreover, HA-Kosloff ALID turns out to be more precise than HA-PML when the time step size increases in the absorbing layers.

Results of 2D elastodynamics problems obtained from HA-Kosloff ALID have been compared with HA-Rayleigh ALID and HA-PML. HA-Kosloff ALID turns out to be a relevant tool for easily modelling the wave propagation in an unbounded domain. Its implementation in the finite element context is very easy, it behaves better than the HA-Rayleigh ALID and it requires less CPU time than a PML formulation. Another advantage of the HA-Kosloff ALID with respect to the HA-PML is its straightforward extension to three-dimensional elastodynamics problems. Future works are in progress to compare the different approaches in complex 3D soil-structure interaction problems.

REFERENCES

[1] Bettess P. Infinite elements. International Journal for Numerical Methods in Engineering 1977; 11: 53–64.

[2] Houmat A. Mapped infinite p-element for two-dimensional problems of unbounded domains. Computers and Geotechnics 2008; 35; 608-615.

[3] Enquist B and Majda A. Absorbing boundary conditions for the numerical simulation of waves. Mathematics of Computation 1977; 31: 629–651.

[4] Bérenger JP. A perfectly matched layer for the absorption of electromagnetic waves. Journal of Computational Physics 1994; 114:185-200.

[5] Chew WC and Liu QH. Perfectly matched layers for elastodynamics: a new absorbing boundary condition. Journal of Computational Acoustics 1996; 4:341–359.

[6] Collino F, Tsogka C. Application of the perfectly matched absorbing layer model to the linear elastodynamic problem in anisotropic heterogeneous media. Geophysics 2001; 66 (1): 294–307.

[7] Basu U and Chopra A. Perfectly matched layers for time-harmonic elastodynamics of unbounded domains: theory and finite-element implementation. Computer Methods in Applied Mechanics and Engineering 2003; 192; 1337-1375.

[8] Basu U and Chopra A. Perfectly matched layers for transient elastodynamics of unbounded domains. International Journal for Numerical Methods in Engineering 2004; 59: 1039–1074.

[9] Basu U. Explicit finite element perfectly matched layer for transient three-dimensional elastic waves. International journal for numerical methods in engineering 2009; 77:151–176.

[10] Hallquist JO, LS-DYNA Keyword User's Manual, Version 971. Livermore Software Technology Corporation: Livermore 2007.

[11] Mamie J, Kikstra WP. DIANA User's Manual, Version10.1. DIANA FEA BV 2016.

[12] Semblat JF, Lenti L, and Gandomzadeh A. A simple multi-directional absorbing layer method to simulate elastic wave propagation in unbounded domains. International Journal for Numerical Methods in Engineering 2011; 85: 1543–1563.

[13] Rajagopal P, Drozdz M, Skelton EA, Lowe MJS, and Craster RV. On the use of the absorbing layers to simulate the propagation of elastic waves in unbounded isotropic media using commercially available finite element packages. NDT and E International 2012; 51: 30–40.

[14] Zafati E, Brun M, Djeran-Maigre I, and Prunier F, Multi-directional and multi-time step absorbing layer for unbounded domain. Comptes Rendus Mécanique 2014;342: 539–557.

[15] Zafati E, Brun M, Djeran-Maigre I, and Prunier F. Design of an efficient multi-directional explicit/implicit Rayleigh absorbing layer for seismic wave propagation in unbounded domain using a strong form formulation. International Journal for Numerical Methods in Engineering 2015; 106: 83–112.

[16] Kosloff D, and Kosloff R. Absorbing boundaries for wave propagation problems. Journal of Computational Physics 1986; 63:363-376.

[17] Carcione JM, Kosloff D. Representation of matched-layer kernels with viscoelastic mechanical models. International Journal of Numerical Analysis and Modeling 2013; 10; 221–232.

[18] ABAQUS v6.13 Abaqus Analysis User's Guide 2013.

[19] Combescure A, and Gravouil A. A numerical scheme to couple subdomains with different time-steps for predominantly linear transient analysis. Computer Methods in Applied Mechanics and Engineering 2002; 191:1129–1157.

[20] Gravouil A, and Combescure A. A multi-time-step explicit–implicit method for non-linear structural dynamics. International Journal for Numerical Methods in Engineering 2001; 50: 199–225.

[21] Brun M, Gravouil A, Combescure A, Limam A. Two FETI-based heterogeneous time step coupling methods for Newmark and α-schemes derived from the energy method. Computer Methods in Applied Mechanics and Engineering 2015; 283: 130–176.

[22] Brun M, Zafati E, Djeran-Maigre I, and Prunier F. Hybrid asynchronous perfectly matched layer for seismic wave propagation in unbounded domains. Finite Elements in Analysis and Design 2016;122: 1–15.

[23] Newmark NM. A method of computation for structural dynamics. Journal of the Engineering Mechanics Division (ASCE) 1959; 85: 67–94.

[24] Lamb H. Proceedings of the 38th Royal Society of London 1903; 72: 128–130.